PROCEEDINGS OF SCIENCE

Measuring atmospheric neutrino oscillations with KM3NeT/ORCA6

V. Carretero[a,*] **on behalf of the KM3NeT Collaboration**

[a] *IFIC (UV-CSIC),*
Carrer del Catedràtic José Beltrán Martinez, 2, 46980, Valencia, Spain

E-mail: vcarretero@km3net.de

The KM3NeT Collaboration is constructing two water-Cherenkov neutrino detectors at the bottom of the Mediterranean Sea: ARCA, which is designed for neutrino astronomy in the TeV to PeV range, and ORCA, optimised for GeV neutrino detection. The ORCA detector will comprise 115 string-like vertical Detection Units arranged in a cylindrical array. Its main objectives are to determine the neutrino mass ordering and measuring atmospheric neutrino oscillations. During 2020 and 2021, an early configuration of the detector with six lines was in operation. A high-purity neutrino sample covering 433 kton-years of exposure was extracted using optimised reconstruction algorithms and machine learning classifiers. In this contribution, the measurement of the neutrino oscillation parameters $\sin^2\theta_{23} = 0.51^{+0.06}_{-0.07}$ and $\Delta m^2_{31} = 2.14^{+0.36}_{-0.25} \cdot 10^{-3}\text{eV}^2$, as well as the sensitivity to determine the neutrino mass ordering based on this data sample, will be presented.

38th International Cosmic Ray Conference (ICRC2023)
26 July - 3 August, 2023
Nagoya, Japan

*Speaker

PoS(ICRC2023)996

1. Introduction

KM3NeT is a research infrastructure for neutrino experiments located on the seabed of the Mediterranean Sea and currently undergoing construction [1]. The infrastructure comprises two detectors that use the same technology but are designed to achieve distinct physics objectives based on their respective spatial configurations. ARCA (Astroparticle Research with Cosmics in the Abyss) is being installed at the KM3NeT-It site, situated 100 km off the coast of Sicily near Capo Passero, Italy, at a depth of 3500 m. ARCA is dedicated to the search for high-energy neutrinos originating from astrophysical sources. ORCA (Oscillation Research with Cosmics in the Abyss) is being built near the coast of Toulon, France, positioned 40 km offshore at a depth of 2500 m. The primary objective of ORCA is to investigate the Neutrino Mass Ordering (NMO) by detecting the neutrino flux generated in the Earth's atmosphere [2]. With a planned instrumented volume of about one cubic kilometer of seawater, ARCA will encompass a mass of one gigaton, while ORCA will cover approximately 7 megatons.

The detection system of ORCA consists of Digital Optical Modules (DOMs) which are pressure-resistant glass spheres housing 31 photomultiplier tubes (PMTs) and corresponding readout electronics [3]. These DOMs are arranged along vertical flexible strings called Detection Units (DUs), anchored to the sea floor and maintained in a vertical position through the buoyancy of the DOMs and a submerged buoy at the top. ORCA will comprise 115 DUs, each equipped with 18 DOMs, with a vertical spacing of 9 m and a horizontal separation of about 20 m. Currently, 18 DUs have been deployed, while the presented results correspond to the initial data acquired using the configuration with 6 DUs referred to as ORCA6.

The ORCA detector employs the Cherenkov effect as its detection principle. Charged particles exceeding the local speed of light induce Cherenkov radiation, which is then registered by the DOMs. This mechanism allows for the reconstruction of interaction parameters, including the interaction vertex, and event topology. By harnessing these capabilities, ORCA enables the exploration of the neutrino properties. Notably, the resulting event topology exhibits distinct light emission characteristics appearing as track-like patterns for GeV muons produced in ν_μ-CC interactions and shower-like patterns for other neutrino channels.

2. Data taking and selection

The ORCA detector has been continuously measuring in the deep sea since mid-2019, while it was extended. From January of 2020 to November 2021, the detector was taking data with a 6-DU configuration. A run selection has been applied to ensure strict data quality criteria resulting in a total of 510 days of data. The time distribution of the exposure is shown in figure 1 in terms of kton-years, taking into account the instrumented volume of seawater, which is corrected by removing non-working PMTs and PMTs with very high rates induced by enviromental optical background. The current dataset corresponds to 433 kton-years. A previous preliminary analysis was carried out with a part of this dataset, in particular using a sample equivalent to 296 kton-years [4]. Several improvements have been made in the selection and analysis with respect to the previous analysis: shower reconstruction was added, selection is now based in machine learning algorithms and energy reconstruction was improved.

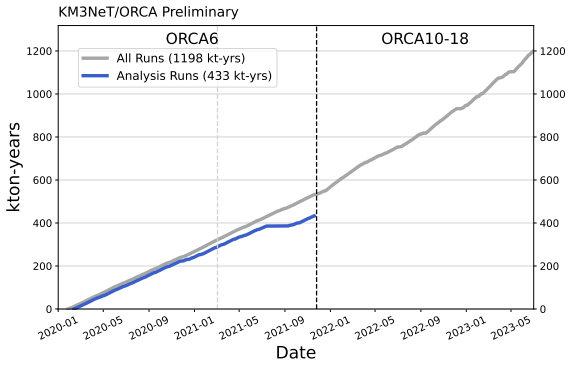

Figure 1: Detector exposure shown as a cumulative livetime as a function of time and configuration in units of kton-years.

The overwhelming majority of recorded events in ORCA are atmospheric muons and pure noise, which have to be rejected in the selection process. To remove these events, first selection is applied by requesting a direction reconstruction with a high quality score, a number of triggered hits above a certain threshold and the reconstructed direction to be up-going, since no atmospheric muons are expected in the up-going direction. A Boosted Decision Tree (BDT) machine learning algorithm is then used to assign particle identification scores to the events that allow to remove remaining atmospheric muons and to discriminate between the two possible event topologies: track-like events and shower-like events. To this end, two scores are calculated which will be called atmospheric muon score and track score, respectively.

After implementing that pre-selection and excluding events with high muon scores, the remaining events are initially categorised into two classes based on the track score: tracks and showers. Subsequently, the track class is further divided into two subclasses using the muon score, which serves as a quality parameter to distinguish well-reconstructed tracks from poorly reconstructed tracks that may be misidentified as atmospheric muons. As a result, three distinct classes of events are formed: High Purity Tracks, Low Purity Tracks, and Showers.

To refine the event selection, an additional selection is applied to the reconstructed energy, but with different thresholds for the shower and track classes. Events with a reconstructed energy exceeding 1 TeV for showers and above 100 GeV for tracks are removed. This specific threshold is employed to mitigate the impact of the migration of high-energy events (above 10 TeV) that are not simulated. Based on this selection process, a total of 5830 events are expected from Monte-Carlo (MC) simulations to meet the criteria while a total of 5828 events were actually observed.

Figure 2 displays the compatibility of the data and MC simulations for the described selection process for both scores. Pre-selection is applied to both data and MC distributions. The additional cut on the muon score to reject the atmospheric muon background is already applied in the track score distribution.

The MC distributions are constructed using events generated with gSeaGen [5] and MUPAGE [6], followed by propagation, triggering, and reconstruction using custom KM3NeT software. MC distributions are simulated with oscillation parameters based on NuFit 5.0 [7] (with Super-Kamiokande data) and normal ordering (NO). The measured data and the modelled MC exhibit

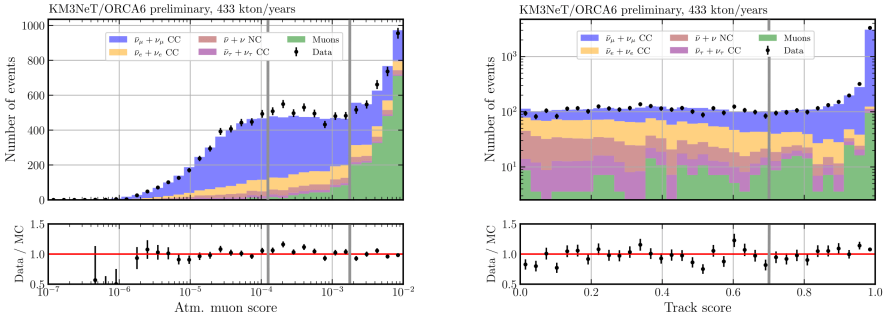

Figure 2: Data/MC distributions as a function of the BDT score, atmospheric muon score (left) and track score (right). Pre-selection is applied to both distributions, an additional cut to remove events with atmospheric muon score higher than $1.8 \cdot 10^{-3}$ is applied. Both show an excellent agreement of data and MC.

good agreement for all the distributions.

3. Analysis

The analysis is based on 2-dimensional distributions of the reconstructed energy and reconstructed cosine of the zenith angle for each of the three event classes. These distributions are obtained through the implementation of Swim [8], an analysis framework developed for KM3NeT which employs MC simulations to model the detector response. The true energy and zenith angle distributions are calculated for each (anti)neutrino interaction type by taking into account cross sections, neutrino fluxes, the interaction volume, and the oscillation probabilities.

Neutrinos are simulated across a wide true energy range, from 1 GeV to 10 TeV, and from all directions. However, only reconstructed up-going directions are used for the analysis, with 10 bins in the reconstructed cosine of the zenith angle. The range of reconstructed energies spans from 2 to 1000 GeV, employing 15 non-equally spaced bins chosen in a way to ensure sufficient statistics per bin. Note that the 15th bin, ranging from 100 to 1000 GeV, exclusively contains shower events, as tracks with reconstructed energies above 100 GeV are rejected.

To account for the detector resolution, a response matrix which is evaluated by reconstructing MC events is employed. This matrix establishes the relationship between the true and reconstructed variables utilised in the analysis. For each interaction channel ν_x and classification i, a 4-dimensional response matrix $R^{[\nu_x \to i]}(E_{\text{true}}, \theta_{\text{true}}, E_{\text{reco}}, \theta_{\text{reco}})$ is defined. Each entry within the matrix represents the detection efficiency, classification, and reconstruction probability for a given bin of true energy and zenith angle $(E_{\text{true}}, \theta_{\text{true}})$. The number of reconstructed events for a given class i is determined by multiplying the expected number of interacting events with these corresponding efficiencies.

$$n^i_{\text{reco}}(E_{\text{reco}}, \theta_{\text{reco}}) = \sum_x n^x_{\text{int}}(E_{\text{true}}, \theta_{\text{true}}) \times R^{[\nu_x \to i]}(E_{\text{true}}, \theta_{\text{true}}, E_{\text{reco}}, \theta_{\text{reco}}), \tag{1}$$

The resulting effective mass for different neutrino flavours and interaction types is shown in figure 3 as a function of neutrino energy. Selection cuts are applied. The effective masses continue

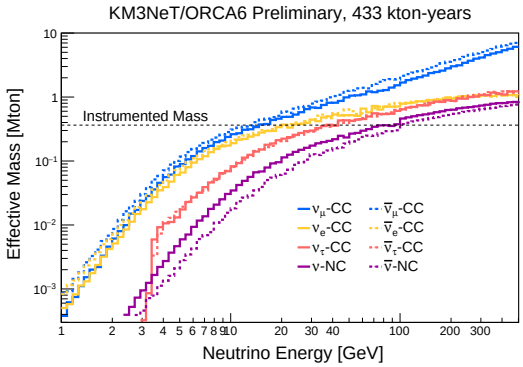

Figure 3: Effective mass for different neutrino flavours and interaction types as a function of the true neutrino energy. Selection cuts are applied. The ORCA6 instrumented mass is shown with a vertical line.

growing as energy grows due to the contribution of events starting outside of the instrumented volume.

The analysis procedure to constrain the oscillation parameters is based on the maximisation of a binned likelihood for the 2-dimensional distribution of events in $\log_{10}(E_{\text{reco}}/\text{GeV})$ and $\cos\theta_{\text{reco}}$, comparing the observed data to a model prediction. The sensitivities are computed using the Asimov approach, in which the observed data is replaced by a representative dataset using the expected values of the null hypothesis for each bin [9]. This analysis is not sensitive to θ_{13}, θ_{12}, Δm^2_{21} and δ_{CP}, so they are fixed to the NuFit 5.0 [7] values. The log-likelihood is modelled as a combination of Poisson distributions for the expected number of events in each bin and Gaussian distributions associated with the nuisance parameters:

$$-2\log L(\vec{\theta}) = \min_{\vec{\epsilon}} \left\{ 2\sum_{i,j}\left[(N_{ij}^{\text{mod}}(\vec{\theta};\vec{\epsilon}) - N_{ij}^{\text{dat}}) + N_{ij}^{\text{dat}} \log\left(\frac{N_{ij}^{\text{dat}}}{N_{ij}^{\text{mod}}(\vec{\theta};\vec{\epsilon})} \right) \right] + \right. \\ \left. + \sum_k \left(\frac{\epsilon_k - \langle \epsilon_k \rangle}{\sigma_k} \right)^2 \right\}. \tag{2}$$

N_{ij}^{mod} and N_{ij}^{dat} represent the number of reconstructed events in bin (i,j) expected by the model and the number of observed events, respectively. The parameters of interest, $\vec{\theta}$, are θ_{23} and Δm^2_{31} in the standard oscillation analysis. The rest of the oscillation parameters is kept fixed. The parameters of the model that characterise the distributions $(\vec{\epsilon})$ are composed by nuisance parameters which are related to systematic uncertainties. Some of these parameters are constrained with priors representing constraints from other experiments. Specifically:

1. Normalisations: the overall normalisation as well as the relative normalisations of the High Purity Track and Shower classes are allowed to vary with no constraints. A 20% prior uncertainty is applied to the normalisation of neutral current (NC) and τ-CC events. At high energies, further approximations are included in the light propagation simulation in KM3NeT/ORCA. A 50% relative normalisation uncertainty is applied to events simulated in this regime.

2. Flux: the spectral index of the neutrino flux energy distribution, as $\phi \times E^s$, is allowed to vary from $s = 0$ with a standard deviation of 0.3. The ratio of electron neutrinos to electron antineutrinos is allowed to vary with a 7% prior uncertainty. The ratio of muon neutrinos to muon antineutrinos is allowed to vary with a 5% prior uncertainty. The ratio of muon neutrinos to electron neutrinos is allowed to vary with a 2% prior uncertainty. The ratio of vertical to horizontal neutrinos, introduced as $1 + r_{\mathrm{h/v}} \cos\theta$, is allowed to vary from $r_{\mathrm{h/v}} = 0$ with a standard deviation of 0.02.

3. The absolute energy scale of the detector is allowed to vary with a 9% prior uncertainty. The energy scale is related to the uncertainty on water optical properties and on the knowledge of the PMT efficiencies.

4. Results

The ORCA6 dataset has been studied to determine the neutrino oscillation parameters. Specifically, the focus in this section is on constraining the oscillation parameters Δm^2_{31} and θ_{23}.

The model is fitted to the dataset using 2-dimensional histograms on the reconstructed energy and direction, as illustrated in figure 4. 5 shows the results of the fit transformed to the L/E (path length over neutrino energy) ratio and normalised with respect to the "non-oscillations" hypothesis for illustration purposes.

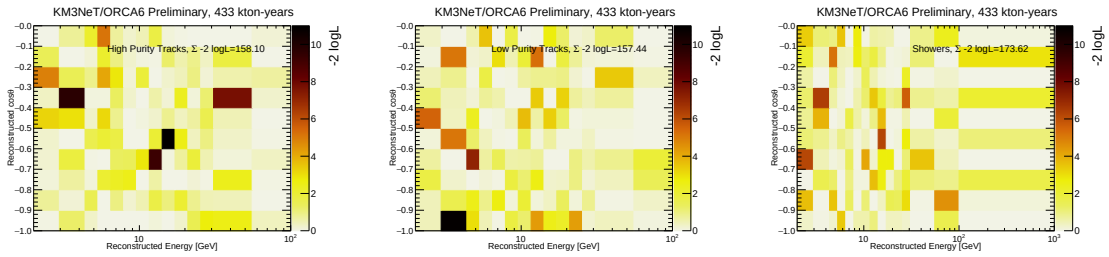

Figure 4: Negative log-likelihood landscape as a function of the reconstructed cosine of the zenith angle and energy for the three classes, High Purity Tracks (left), Low Purity Tracks (middle) and Showers (right). Total negative log-likelihood is reported per class.

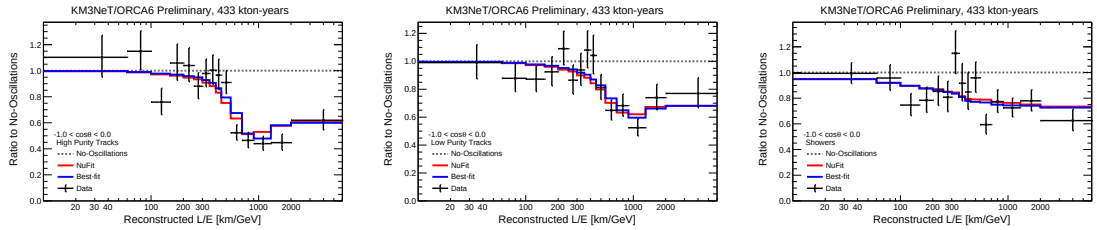

Figure 5: Ratio to non-oscillations as a function of the reconstructed path length over reconstructed neutrino energy, L/E, for data (black), the best-fit (blue), and NuFit (red) for the three classes: High Purity Tracks (left), Low Purity Tracks (middle), and Showers (right). Non-oscillations and NuFit hypotheses are computed taking the best-fit and fixing the oscillation parameters to the corresponding hypothesis.

The fit deviates from the expectations derived from the NuFit model by less than 1σ. There is a preference for NO over IO: $-2\log\left(\frac{L_{NO}}{L_{IO}}\right) = 0.9$. The best-fit values for the parameters are $\sin^2\theta_{23} = 0.51^{+0.06}_{-0.07}$ and $\Delta m^2_{31} = 2.14^{+0.25}_{-0.36} \cdot 10^{-3}\text{eV}^2$.

The space of oscillation parameters has been scanned and profiled in terms of the negative log-likelihood, in order to provide 1-dimensional scans and a 2-dimensional contour of the sensitivity of the ORCA detector for neutrino oscillations. Figure 6 shows the 1-D scans of the profiled likelihood with 68% and 90% CL bands, computed by generating pseudo-experiments with the best-fit values of oscillation and nuisance parameters. The 90% CL contour for both parameters constrained simultaneously is shown in figure 7 in comparison to other experiments.

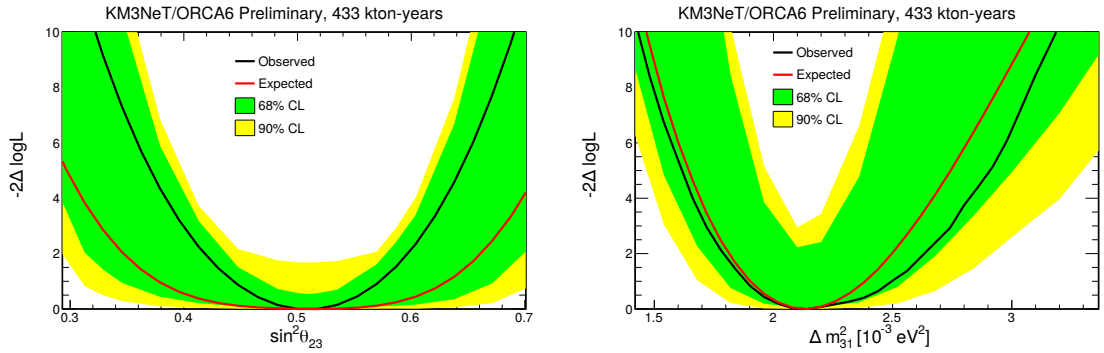

Figure 6: Profiled negative log-likelihood scan of the oscillation parameters, $\sin^2\theta_{23}$ (left) and Δm^2_{31} (right). Observed limits are compatible within the 68% CL bands.

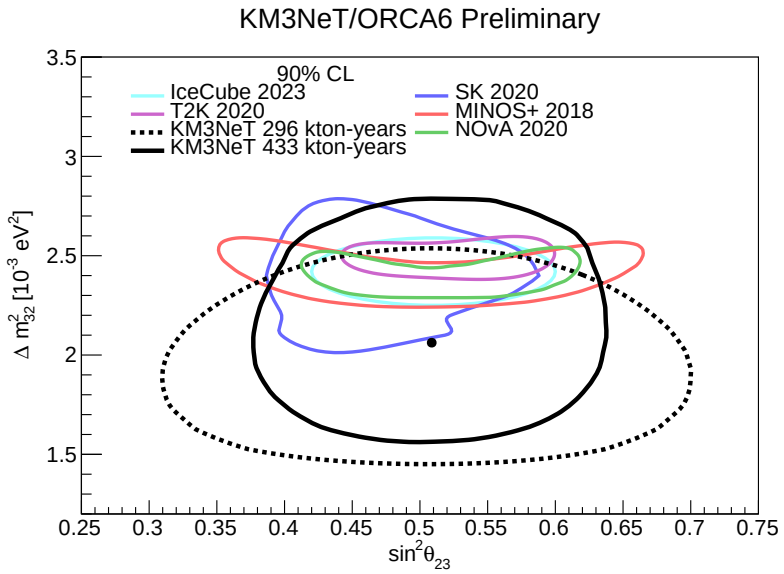

Figure 7: Contour at 90% CL of ORCA6 for the oscillation parameters $\sin^2\theta_{23}$ and Δm^2_{31} compared with other experiments. A previous result obtained with a first ORCA6 dataset is included [4].

Figure 8 shows the effect of the different systematic uncertainties. The impact is computed comparing the nominal best-fit value of θ_{23} and Δm^2_{31} with the result of the fit when fixing the considered nuisance parameter shifted by $\pm$ its post-fit uncertainty. Black dots with error bars

represent the pulls of the parameter's best-fit. The error bars are computed as the post-fit uncertainty divided by the pre-fit uncertainty (priors). If the parameter was unconstrained, the pull is computed based on the post-fit uncertainty and the error bar is 1.

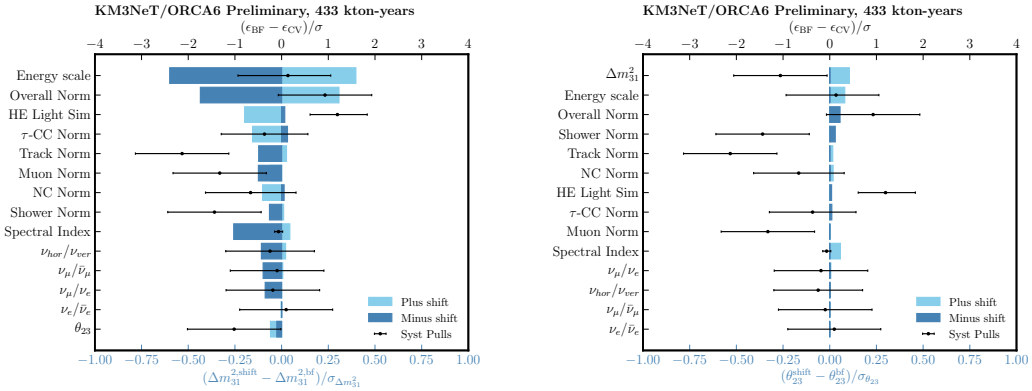

Figure 8: Impact of the different systematic parameters computed as a shift in the parameter of interest, Δm^2_{31} (left) and θ_{23} (right) when the nuisance parameter is shifted and fixed. Systematic pulls are reported as black dots.

This test provides insights into the parameter correlations. Specifically, Δm^2_{31} exhibits strong correlations with the systematic due to energy scale, energy spectral index, and the overall normalisation. On the other hand, correlations involving θ_{23} are generally small, although non-negligible contributions are observed from the energy scale, Δm^2_{31}, and the overall normalisation nuisance parameters.

5. Conclusions

With only 5% of its final configuration, the ORCA detector starts to contribute to the measurement of atmospheric neutrino oscillations. The best fit values for the parameters are $\sin^2\theta_{23} = 0.51^{+0.06}_{-0.07}$ and $\Delta m^2_{31} = 2.14^{+0.36}_{-0.25} \cdot 10^{-3}\text{eV}^2$ with a preference for NO: $-2\log\left(\frac{L_{NO}}{L_{IO}}\right) = 0.9$. The detector deployment is progressing continuously and these measurements will gain in precision as the detector volume increases and the reconstruction and selection efficiencies are improved.

References

[1] KM3NeT Collaboration, DOI: 10.1088/0954-3899/43/8/084001
[2] KM3NeT Collaboration, DOI: 10.1140/epjc/s10052-021-09893-0
[3] KM3NeT Collaboration, DOI: 10.1088/1748-0221/17/07/P07038
[4] L. Nauta et al, DOI: 10.22323/1.395.1123
[5] KM3NeT Collaboration, DOI: 10.1016/j.cpc.2020.107477
[6] G. Carminati et al., DOI: 10.1016/j.cpc.2008.07.014
[7] I. Esteban et al, DOI: 10.1007/JHEP09(2020)178
[8] S. Bourret, https://theses.hal.science/tel-02491394
[9] G. Cowan et al. DOI: 10.1140/epjc/s10052-011-1554-0

Full Authors List: The KM3NeT Collaboration

S. Aiello[a], A. Albert[b,bd], S. Alves Garre[c], Z. Aly[d], A. Ambrosone[f,e], F. Ameli[g], M. Andre[h], E. Androutsou[i], M. Anguita[j], L. Aphecetche[k], M. Ardid[l], S. Ardid[l], H. Atmani[m], J. Aublin[n], L. Bailly-Salins[o], Z. Bardačová[q,p], B. Baret[n], A. Bariego-Quintana[c], S. Basegmez du Pree[r], Y. Becherini[n], M. Bendahman[m,n], F. Benfenati[t,s], M. Benhassi[u,e], D. M. Benoit[v], E. Berbee[r], V. Bertin[d], S. Biagi[w], M. Boettcher[x], D. Bonanno[w], J. Boumaaza[m], M. Bouta[y], M. Bouwhuis[r], C. Bozza[z,e], R. M. Bozza[f,e], H.Brânzaş[aa], F. Bretaudeau[k], R. Bruijn[ab,r], J. Brunner[d], R. Bruno[a], E. Buis[ac,r], R. Buompane[u,e], J. Busto[d], B. Caiffi[ad], D. Calvo[c], S. Campion[g,ae], A. Capone[g,ae], F. Carenini[t,s], V. Carretero[c], T. Cartraud[n], P. Castaldi[af,s], V. Cecchini[c], S. Celli[g,ae], L. Cerisy[d], M. Chabab[ag], M. Chadolias[ah], A. Chen[ai], S. Cherubini[aj,w], T. Chiarusi[s], M. Circella[ak], R. Cocimano[w], J. A. B. Coelho[n], A. Coleiro[n], R. Coniglione[w] P. Coyle[d], A. Creusot[n], A. Cruz[al], G. Cuttone[w], R. Dallier[k], Y. Darras[ah], A. De Benedittis[e], B. De Martino[d], V. Decoene[k], R. Del Burgo[e], U. M. Di Cerbo[e], L. S. Di Mauro[w], I. Di Palma[g,ae], A. F. Díaz[j], C. Diaz[j], D. Diego-Tortosa[w], C. Distefano[w], A. Domi[ah], C. Donzaud[n], D. Dornic[d], M. Dörr[am], E. Drakopoulou[i], D. Drouhin[b,bd], R. Dvornický[q], T. Eberl[ah], E. Eckerová[q,p], A. Eddymaoui[m], T. van Eeden[r], M. Eff[n], D. van Eijk[r], I. El Bojaddaini[y], S. El Hedri[n], A. Enzenhöfer[d], G. Ferrara[w], M. D. Filipović[an], F. Filippini[t,s], D. Franciotti[w], L. A. Fusco[z,e], J. Gabriel[ao], S. Gagliardini[g], T. Gal[ah], J. García Méndez[l], A. Garcia Soto[c], C. Gatius Oliver[r], N. Geißelbrecht[ah], H. Ghaddari[y], L. Gialanella[e,u], B. K. Gibson[v], E. Giorgio[w], I. Goos[n], D. Goupilliere[o], S. R. Gozzini[c], R. Gracia[ah], K. Graf[ah], C. Guidi[ap,ad], B. Guillon[o], M. Gutiérrez[aq], H. van Haren[ar], A. Heijboer[r], A. Hekalo[am], L. Hennig[ah], J. J. Hernández-Rey[c], F. Huang[d], W. Idrissi Ibnsalih[e], G. Illuminati[s], C. W. James[al], M. de Jong[as,r], P. de Jong[ab,r], B. J. Jung[r], P. Kalaczyński[at,be], O. Kalekin[ah], U. F. Katz[ah], N. R. Khan Chowdhury[c], A. Khatun[q], G. Kistauri[av,au], C. Kopper[ah], A. Kouchner[aw,n], V. Kulikovskiy[ad], R. Kvatadze[av], M. Labalme[o], R. Lahmann[ah], G. Larosa[w], C. Lastoria[d], A. Lazo[c], S. Le Stum[d], G. Lehaut[o], E. Leonora[a], N. Lessing[c], G. Levi[t,s], M. Lindsey Clark[n], F. Longhitano[a], J. Majumdar[r], L. Malerba[ad], F. Mamedov[p], J. Mańczak[c], A. Manfreda[e], M. Marconi[ap,ad], A. Margiotta[t,s], A. Marinelli[e,f], C. Markou[i], L. Martin[k], J. A. Martínez-Mora[l], F. Marzaioli[u,e], M. Mastrodicasa[ae,g], S. Mastroianni[e], S. Miccichè[w], G. Miele[f,e], P. Migliozzi[e], E. Migneco[w], M. L. Mitsou[e], C. M. Mollo[e], L. Morales-Gallegos[u,e], C. Morley-Wong[al], A. Moussa[y], I. Mozun Mateo[ay,ax], R. Muller[r], M. R. Musone[e,u], M. Musumeci[w], L. Nauta[r], S. Navas[aq], A. Nayerhoda[ak], C. A. Nicolau[g], B. Nkosi[ai], B. Ó Fearraigh[ab,r], V. Oliviero[f,e], A. Orlando[w], E. Oukacha[n], D. Paesani[w], J. Palacios González[c], G. Papalashvili[au], V. Parisi[ap,ad], E.J. Pastor Gomez[c], A. M. Păun[aa], G. E. Păvălaş[aa], S. Peña Martínez[n], M. Perrin-Terrin[d], J. Perronnel[o], V. Pestel[ay], R. Pestes[n], P. Piattelli[w], C. Poirè[z,e], V. Popa[aa], T. Pradier[b], S. Pulvirenti[w], G. Quéméner[o], C. Quiroz[l], U. Rahaman[c], N. Randazzo[a], R. Randriatoamanana[k], S. Razzaque[az], I. C. Rea[e], D. Real[c], S. Reck[ah], G. Riccobene[w], J. Robinson[x], A. Romanov[ap,ad], A. Šaina[c], F. Salesa Greus[c], D. F. E. Samtleben[as,r], A. Sánchez Losa[c,ak], S. Sanfilippo[w], M. Sanguineti[ap,ad], C. Santonastaso[ba,e], D. Santonocito[w], P. Sapienza[w], J. Schnabel[ah], J. Schumann[ah], H. M. Schutte[x], J. Seneca[r], N. Sennan[y], B. Setter[ah], I. Sgura[ak], R. Shanidze[au], Y. Shitov[p], F. Šimkovic[q], A. Simonelli[e], A. Sinopoulou[a], M.V. Smirnov[ah], B. Spisso[e], M. Spurio[t,s], D. Stavropoulos[i], I. Štekl[p], M. Taiuti[ap,ad], Y. Tayalati[m], H. Tedjditi[ad], H. Thiersen[x], I. Tosta e Melo[a,aj], B. Trocmé[n], V. Tsourapis[i], E. Tzamariudaki[i], A. Vacheret[o], V. Valsecchi[w], V. Van Elewyck[aw,n], G. Vannoye[d], G. Vasileiadis[bb], F. Vazquez de Sola[r], C. Verilhac[n], A. Veutro[g,ae], S. Viola[w], D. Vivolo[u,e], J. Wilms[bc], E. de Wolf[ab,r], H. Yepes-Ramirez[l], G. Zarpapis[i], S. Zavatarelli[ad], A. Zegarelli[g,ae], D. Zito[w], J. D. Zornoza[c], J. Zúñiga[c], and N. Zywucka[x].

[a] INFN, Sezione di Catania, Via Santa Sofia 64, Catania, 95123 Italy

[b] Université de Strasbourg, CNRS, IPHC UMR 7178, F-67000 Strasbourg, France

[c] IFIC - Instituto de Física Corpuscular (CSIC - Universitat de València), c/Catedrático José Beltrán, 2, 46980 Paterna, Valencia, Spain

[d] Aix Marseille Univ, CNRS/IN2P3, CPPM, Marseille, France

[e] INFN, Sezione di Napoli, Complesso Universitario di Monte S. Angelo, Via Cintia ed. G, Napoli, 80126 Italy

[f] Università di Napoli "Federico II", Dip. Scienze Fisiche "E. Pancini", Complesso Universitario di Monte S. Angelo, Via Cintia ed. G, Napoli, 80126 Italy

[g] INFN, Sezione di Roma, Piazzale Aldo Moro 2, Roma, 00185 Italy

[h] Universitat Politècnica de Catalunya, Laboratori d'Aplicacions Bioacústiques, Centre Tecnològic de Vilanova i la Geltrú, Avda. Rambla Exposició, s/n, Vilanova i la Geltrú, 08800 Spain

[i] NCSR Demokritos, Institute of Nuclear and Particle Physics, Ag. Paraskevi Attikis, Athens, 15310 Greece

[j] University of Granada, Dept. of Computer Architecture and Technology/CITIC, 18071 Granada, Spain

[k] Subatech, IMT Atlantique, IN2P3-CNRS, Université de Nantes, 4 rue Alfred Kastler - La Chantrerie, Nantes, BP 20722 44307 France

[l] Universitat Politècnica de València, Instituto de Investigación para la Gestión Integrada de las Zonas Costeras, C/ Paranimf, 1, Gandia, 46730 Spain

[m] University Mohammed V in Rabat, Faculty of Sciences, 4 av. Ibn Battouta, B.P. 1014, R.P. 10000 Rabat, Morocco

[n] Université Paris Cité, CNRS, Astroparticule et Cosmologie, F-75013 Paris, France

[o] LPC CAEN, Normandie Univ, ENSICAEN, UNICAEN, CNRS/IN2P3, 6 boulevard Maréchal Juin, Caen, 14050 France

[p] Czech Technical University in Prague, Institute of Experimental and Applied Physics, Husova 240/5, Prague, 110 00 Czech Republic

[q] Comenius University in Bratislava, Department of Nuclear Physics and Biophysics, Mlynska dolina F1, Bratislava, 842 48 Slovak Republic

[r] Nikhef, National Institute for Subatomic Physics, PO Box 41882, Amsterdam, 1009 DB Netherlands

[s] INFN, Sezione di Bologna, v.le C. Berti-Pichat, 6/2, Bologna, 40127 Italy

[t] Università di Bologna, Dipartimento di Fisica e Astronomia, v.le C. Berti-Pichat, 6/2, Bologna, 40127 Italy

[u] Università degli Studi della Campania "Luigi Vanvitelli", Dipartimento di Matematica e Fisica, viale Lincoln 5, Caserta, 81100 Italy

[v] E. A. Milne Centre for Astrophysics, University of Hull, Hull, HU6 7RX, United Kingdom

[w] INFN, Laboratori Nazionali del Sud, Via S. Sofia 62, Catania, 95123 Italy
[x] North-West University, Centre for Space Research, Private Bag X6001, Potchefstroom, 2520 South Africa
[y] University Mohammed I, Faculty of Sciences, BV Mohammed VI, B.P. 717, R.P. 60000 Oujda, Morocco
[z] Università di Salerno e INFN Gruppo Collegato di Salerno, Dipartimento di Fisica, Via Giovanni Paolo II 132, Fisciano, 84084 Italy
[aa] ISS, Atomistilor 409, Măgurele, RO-077125 Romania
[ab] University of Amsterdam, Institute of Physics/IHEF, PO Box 94216, Amsterdam, 1090 GE Netherlands
[ac] TNO, Technical Sciences, PO Box 155, Delft, 2600 AD Netherlands
[ad] INFN, Sezione di Genova, Via Dodecaneso 33, Genova, 16146 Italy
[ae] Università La Sapienza, Dipartimento di Fisica, Piazzale Aldo Moro 2, Roma, 00185 Italy
[af] Università di Bologna, Dipartimento di Ingegneria dell'Energia Elettrica e dell'Informazione "Guglielmo Marconi", Via dell'Università 50, Cesena, 47521 Italia
[ag] Cadi Ayyad University, Physics Department, Faculty of Science Semlalia, Av. My Abdellah, P.O.B. 2390, Marrakech, 40000 Morocco
[ah] Friedrich-Alexander-Universität Erlangen-Nürnberg (FAU), Erlangen Centre for Astroparticle Physics, Nikolaus-Fiebiger-Straße 2, 91058 Erlangen, Germany
[ai] University of the Witwatersrand, School of Physics, Private Bag 3, Johannesburg, Wits 2050 South Africa
[aj] Università di Catania, Dipartimento di Fisica e Astronomia "Ettore Majorana", Via Santa Sofia 64, Catania, 95123 Italy
[ak] INFN, Sezione di Bari, via Orabona, 4, Bari, 70125 Italy
[al] International Centre for Radio Astronomy Research, Curtin University, Bentley, WA 6102, Australia
[am] University Würzburg, Emil-Fischer-Straße 31, Würzburg, 97074 Germany
[an] Western Sydney University, School of Computing, Engineering and Mathematics, Locked Bag 1797, Penrith, NSW 2751 Australia
[ao] IN2P3, LPC, Campus des Cézeaux 24, avenue des Landais BP 80026, Aubière Cedex, 63171 France
[ap] Università di Genova, Via Dodecaneso 33, Genova, 16146 Italy
[aq] University of Granada, Dpto. de Física Teórica y del Cosmos & C.A.F.P.E., 18071 Granada, Spain
[ar] NIOZ (Royal Netherlands Institute for Sea Research), PO Box 59, Den Burg, Texel, 1790 AB, the Netherlands
[as] Leiden University, Leiden Institute of Physics, PO Box 9504, Leiden, 2300 RA Netherlands
[at] National Centre for Nuclear Research, 02-093 Warsaw, Poland
[au] Tbilisi State University, Department of Physics, 3, Chavchavadze Ave., Tbilisi, 0179 Georgia
[av] The University of Georgia, Institute of Physics, Kostava str. 77, Tbilisi, 0171 Georgia
[aw] Institut Universitaire de France, 1 rue Descartes, Paris, 75005 France
[ax] IN2P3, 3, Rue Michel-Ange, Paris 16, 75794 France
[ay] LPC, Campus des Cézeaux 24, avenue des Landais BP 80026, Aubière Cedex, 63171 France
[az] University of Johannesburg, Department Physics, PO Box 524, Auckland Park, 2006 South Africa
[ba] Università degli Studi della Campania "Luigi Vanvitelli", CAPACITY, Laboratorio CIRCE - Dip. Di Matematica e Fisica - Viale Carlo III di Borbone 153, San Nicola La Strada, 81020 Italy
[bb] Laboratoire Univers et Particules de Montpellier, Place Eugène Bataillon - CC 72, Montpellier Cédex 05, 34095 France
[bc] Friedrich-Alexander-Universität Erlangen-Nürnberg (FAU), Remeis Sternwarte, Sternwartstraße 7, 96049 Bamberg, Germany
[bd] Université de Haute Alsace, rue des Frères Lumière, 68093 Mulhouse Cedex, France
[be] AstroCeNT, Nicolaus Copernicus Astronomical Center, Polish Academy of Sciences, Rektorska 4, Warsaw, 00-614 Poland

Acknowledgements

The authors acknowledge the financial support of the funding agencies: Agence Nationale de la Recherche (contract ANR-15-CE31-0020), Centre National de la Recherche Scientifique (CNRS), Commission Européenne (FEDER fund and Marie Curie Program), LabEx UnivEarthS (ANR-10-LABX-0023 and ANR-18-IDEX-0001), Paris Île-de-France Region, France; Shota Rustaveli National Science Foundation of Georgia (SRNSFG, FR-22-13708), Georgia; The General Secretariat of Research and Innovation (GSRI), Greece Istituto Nazionale di Fisica Nucleare (INFN), Ministero dell'Università e della Ricerca (MIUR), PRIN 2017 program (Grant NAT-NET 2017W4HA7S) Italy; Ministry of Higher Education, Scientific Research and Innovation, Morocco, and the Arab Fund for Economic and Social Development, Kuwait; Nederlandse organisatie voor Wetenschappelijk Onderzoek (NWO), the Netherlands; The National Science Centre, Poland (2021/41/N/ST2/01177); The grant "AstroCeNT: Particle Astrophysics Science and Technology Centre", carried out within the International Research Agendas programme of the Foundation for Polish Science financed by the European Union under the European Regional Development Fund; National Authority for Scientific Research (ANCS), Romania; Grants PID2021-124591NB-C41, -C42, -C43 funded by MCIN/AEI/ 10.13039/501100011033 and, as appropriate, by "ERDF A way of making Europe", by the "European Union" or by the "European Union NextGenerationEU/PRTR", Programa de Planes Complementarios I+D+I (refs. ASFAE/2022/023, ASFAE/2022/014), Programa Prometeo (PROMETEO/2020/019) and GenT (refs. CIDEGENT/2018/034, /2019/043, /2020/049. /2021/23) of the Generalitat Valenciana, Junta de Andalucía (ref. SOMM17/6104/UGR, P18-FR-5057), EU: MSC program (ref. 101025085), Programa María Zambrano (Spanish Ministry of Universities, funded by the European Union, NextGenerationEU), Spain; The European Union's Horizon 2020 Research and Innovation Programme (ChETEC-INFRA - Project no. 101008324).